Remote Sensing in Ecology and Conservation
Open Access
ZSL LET'S WORK FOR WILDLIFE

ORIGINAL RESEARCH

Mapping with confidence; delineating seagrass habitats using Unoccupied Aerial Systems (UAS)

Natasha K. Nahirnick[1], Luba Reshitnyk[2], Marcus Campbell[2], Margot Hessing-Lewis[2], Maycira Costa[1], Jennifer Yakimishyn[3] & Lynn Lee[4]

[1]Department of Geography, University of Victoria, 3800 Finnerty Road, Victoria, British Columbia, Canada, V8P 5C2
[2]Hakai Institute, PO Box 309, Heriot Bay, British Columbia, Canada, V0P 1H0
[3]Pacific Rim National Park Reserve of Canada, PO Box 280, Ucluelet, British Columbia, Canada, V0R 3A0
[4]Gwaii Haanas National Marine Conservation Area Reserve and Haida Heritage Site, PO Box 37, Queen Charlotte British Columbia, Canada, V0T 1S0

Keywords
British Columbia, drone, marine habitat mapping, nearshore, seagrass, UAS, UAV, *Zostera marina*

Correspondence
Natasha K. Nahirnick, Department of Geography, University of Victoria, 3800 Finnerty Road, Victoria, BC, Canada V8P 5C2. Tel: +1 778 678 2668;
E-mail: kadence@uvic.ca

Funding Information
This research was jointly supported by the Tula Foundation, Parks Canada, University of Victoria and Mitacs (Grant #IT07414)

Editor: Ned Horning
Associate Editor: Dimitris Poursanidis

Received: 29 June 2018; Revised: 7 September 2018; Accepted: 12 October 2018

doi: 10.1002/rse2.98

Abstract

There is growing interest in the use of Unoccupied Aerial Systems (UAS) for mapping and monitoring of seagrass habitats. UAS provide flexibility with timing of imagery capture, are relatively inexpensive, and obtain very high spatial resolution imagery compared to imagery acquired from sensors mounted on satellite or piloted aircraft. However, research to date has focused on UAS applications for exposed intertidal areas or clear tropical waters. In contrast, submerged seagrass meadows in temperate regions are subject to high cloud cover and water column turbidity, which may limit the application of UAS imagery for coastal habitat mapping. To test the constraints on UAS seagrass mapping, we examined the effects of five environmental conditions at the time of UAS image acquisition (sun angle, tidal height, cloud cover, Secchi depth and wind speed) and five site characteristics (eelgrass patchiness and density, presence and density of non-eelgrass submerged aquatic vegetation, sediment tone, eelgrass deep edge and site exposure) at 26 eelgrass (*Zostera marina*) monitoring sites in British Columbia, Canada. Eelgrass was delineated in UAS orthomosaics using object-based image analysis, combining image segmentation with manual classification. Each site was ranked according to the analysts' confidence in the delineated eelgrass. Robust Linear Regression revealed sun angle and '*theoretical visibility*' (an aggregate of tidal height, Secchi depth, and eelgrass deep edge conditions) to be the most important variables affecting mapping confidence. In general, ideal environmental conditions to obtain high confidence eelgrass mapping included: (1) sun angles below 40°; (2) positive theoretical visibility with Secchi depths >5 m; (3) cloud cover conditions of <10% or >90%; and (4) wind speeds less than 5 km h^{-1}. Additionally, high mapping confidence was achieved for sites with dense, continuous, and homogeneous eelgrass meadows. The results of this analysis will guide implementation of UAS mapping technologies in coastal temperate regions.

Introduction

Seagrass meadows are globally recognized as vital coastal ecosystems, providing key ecological services, including: wildlife habitat, sediment retention, wave and current buffering and nutrient cycling (Costanza et al. 1997; Beck et al. 2001; Hansen and Reidenbach 2013; Plummer et al. 2013). Seagrasses are considered biological sentinels of anthropogenic impacts in coastal areas and global loss of seagrasses has highlighted the need to monitor, conserve and restore these important ecosystems (Orth et al. 2006). Effective management of seagrass landscapes need to consider the spatial extent and configuration of seagrass meadows to understand how they support biodiversity across seascapes (Bostrom et al. 2011). Consequently, assessing the spatial coverage of seagrasses and

monitoring changes over time in seagrass bed dynamics is imperative to nearshore conservation, restoration and management in an era of increasing coastal human populations and associated anthropogenic impacts (Short and Wyllie-Echeverria 1996; Larkum et al. 2007).

Remotely sensed aerial or satellite optical imagery have been used successfully to assess the spatial distribution and spatio-temporal changes in seagrass habitats (Lathrop et al. 2006; O'Neill and Costa 2013; Hogrefe et al. 2014; Reshitnyk et al. 2014). Remote sensing techniques are advantageous as they can capture the spatial extent of seagrass over large geographic areas more efficiently than ground-based assessment methods (Hossain et al. 2015; Klemas 2016). However, at finer spatial resolutions, satellite and airborne imagery may be prohibitively expensive for site-scale mapping efforts, and further, these platforms have limited flexibility for image acquisition under specific environmental conditions necessary for optimal mapping of submerged habitats (e.g., low tide, cloud-free) (O'Neill and Costa 2013; Reshitnyk et al. 2014).

As an alternative remote sensing tool, near-field remote sensing, using Unoccupied Aerial Systems (UAS) (Johnston 2019), commonly referred to as drones, are becoming popular platforms for spatial assessment of ecological phenomena (e.g., Anderson and Gaston 2013; Klemas 2015; Manfreda et al. 2018; Singh and Frazier 2018). These remote sensing platforms have the capacity for acquiring imagery of very fine spatial resolution (0.01–5 cm), have increased flexibility for image acquisition, and generally have lower operational costs. For seagrass habitat assessment, very fine resolution UAS imagery has been effective for density coverage mapping and detecting changes in small patch and landscape features that would not be possible with satellite or aerial photography (Barrell and Grant 2015; Duffy et al. 2018). However, the application of UAS for mapping and monitoring submerged aquatic vegetation (SAV) has been limited by the challenges associated with the water overlying target benthic features and the environmental conditions at the time of image acquisition (Nahirnick et al. in press). As such, most research has been confined to clear shallow tropical waters (Ventura et al. 2016; Casella et al. 2017) or small subsets of exposed intertidal seagrass beds in temperate regions (Barrell and Grant 2015; Duffy et al. 2018).

Wider adoption of UAS technology for seagrass mapping requires a better understanding of both the role of environmental conditions and the site characteristics that affect mapping reliability. Temperate regions test the limits of conditions permissive to UAS mapping of submerged habitat because they are subject to periods of reduced water clarity (i.e., high turbidity) related to terrestrial inputs and phytoplankton blooms (Babin et al., 2003; Dekker et al., 2006) . In addition, higher frequency of cloud cover and inclement weather (e.g., rain, wind, fog), common in temperate systems, can limit acquisition of high quality imagery, both spatially and temporally (Dobson et al., 1996; Finkbeiner et al. 2001). Site-specific characteristics also influence the effectiveness of remotely sensed mapping due to the size, shape and density of seagrass beds, and their potential confusion with other SAV or background sediments (Pasqualini et al. 1997; Lathrop et al. 2006; Knudby and Nordlund 2011; O'Neill and Costa 2013; Reshitnyk et al. 2014). The aggregate challenges posed by both the water column, atmospheric conditions and seagrass bed characteristics, may interact to impact the quality, accuracy and confidence in seagrass UAS mapping.

To understand the limitations to UAS mapping of seagrass extent across a temperate coastal region, we assessed both (1) environmental conditions during imagery acquisition, and (2) site-specific characteristics of the seagrass bed. We determined the most important variables predicting seagrass mapping confidence. Further, we reviewed the role of each variable separately to provide guidance for implementation of UAS seagrass mapping. Given the high frequency of overcast conditions and decreased water clarity in temperate regions, we predicted that both cloud cover and turbidity would have the greatest effect on achieving accurate seagrass UAS mapping. In addition, we hypothesized that water column parameters, such as turbidity, would interact with tide height and seagrass distribution to impact our ability to detect the eelgrass deep edge. Furthermore, we anticipated that eelgrass bed characteristics, including density and patchiness and the presence of non-eelgrass SAV, would affect mapping confidence.

Materials and Methods

Study sites

UAS flights were conducted at 26 sites in four regions across the west coast of British Columbia (BC), Canada, during the summer of 2017 (Fig. 1). These four regions represent a large latitudinal gradient (48.8° to 52.6°) in seagrass distribution in BC, are the focus of long-term eelgrass monitoring efforts, and encompass variable site characteristics subject to a gradient in environmental conditions. The four regions include: (1) Broken Group Islands, Pacific Rim National Park Reserve, southwest coast (eight sites); (2) Gulf Islands National Park Reserve, southeast coast (three sites); (3) Gwaii Haanas National Park Reserve, National Marine Conservation Area Reserve and Haida Heritage Site (GHNMCA) on Haida Gwaii, north coast (nine sites); (4) the Hakai-Luxvbalis

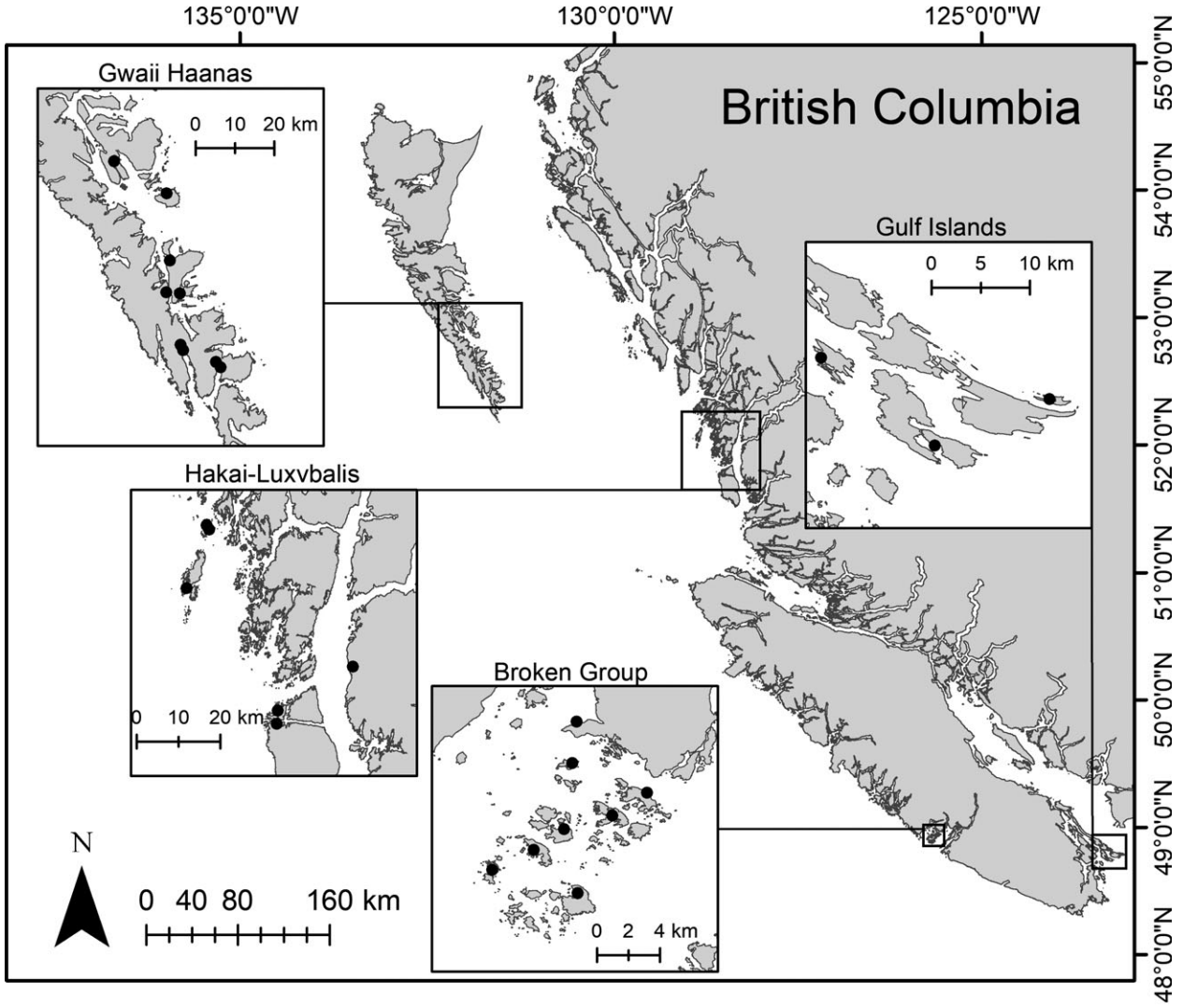

Figure 1. Location of eelgrass mapping sites in each of four study regions in British Columbia: Gwaii Haanas, Haida Gwaii, north coast; Hakai-Luxvbalis, central coast; Gulf Islands, south-east coast; Broken Group, Pacific Rim National Park and south-west coast

Conservancy, central coast (six sites). UAS and towed video data were collected concurrently with eelgrass monitoring surveys conducted by the Hakai Institute and Parks Canada.

UAS image collection

Imagery was collected across the eelgrass growing season in the Pacific Northwest region (Phillips 1984): June – August 2017, during morning low tides with no rain, and within wind speeds safe for UAS flight (<35 km h^{-1}). Prior to each flight, ground control points (GCPs) were distributed evenly throughout the survey area (Martínez-Carricondo et al. 2018). The coordinates of each GCP were recorded using a Topcon GR5 GPS unit with positional accuracy of <1.0 m. GCPs improve the positional accuracy of the imagery by tying the imagery to a known geographic reference system. A DJI Phantom 3 Professional UAS was used to collect imagery. This model has an onboard camera with a 1/2.3 inch CMOS sensor which captures 12 megapixel images (.jpeg format) and a f/2.8 lens with a 94° field of view. Automated flights were conducted within the MapPilot application with 75% overlap on both axes, and altitude of flight ranged from 80 to 120 m depending on the size of the site. Images were captured under continuous flight (not pausing during image capture) with flight speed typically less than 5 m s^{-1} to minimize image blur. The distance between images was calculated automatically within the flight application based on the overlap parameters at a specific

flight elevation. Field data describing environmental conditions were collected concurrently (Table 1), including Secchi depth (m) in 2–4 locations (positive value from sea surface to maximum visible depth), cloud cover (%) with sky photos, and wind speed (km h^{-1}) using a handheld anemometer. Time was recorded to derive tidal height and sun angle. Environmental condition data collected in the field are reported for each site in Appendix A1.

Ground truth data

Towed underwater video surveys (Deep Blue Pro, Ocean Systems Inc.) were conducted at each site to collect ground-reference data. A survey-grade GPS (Topcon GR5) was used to collect positional data for the towed data (<1.0 m positional accuracy). The camera operator maintained the camera at an oblique angle 1–2 m above the sea floor by monitoring the live video feed. Depending on the size of the site, between two and six transects were collected at each site. Tows were conducted perpendicular to the shore to capture the deep and shallow edges of the eelgrass meadows. Video collection was conducted on high tides as close as possible to UAS image collection to minimize potential differences between site characteristics through time.

Habitat type was categorized by analysis of underwater video. Benthic composition was recorded every four seconds and classified into five major benthic habitat types: (1) green algae (Chlorophyta); (2) brown algae (Phaophycae); (3) red algae (Rhodophyta); (4) eelgrass (*Z. marina*); and (5) unvegetated substrate (sand, cobble, gravel, wood debris) (classification scheme from Reshitnyk et al. (2014), adapted from Green et al. (2000)). Each non-eelgrass SAV (i.e., algal) cover type was classified as sparse (<50% seafloor coverage) or dense (>50% seafloor coverage), and eelgrass was classified into four density categories: very sparse (5–20% cover), sparse (20–60% cover), moderately dense (60–80% cover), and very dense (80–100% cover) (Fig. 2). In the case of mixed vegetation frames, both eelgrass and the non-eelgrass SAV were classified, but the frame was treated as eelgrass present.

Derived site and environmental characteristics

In addition to the variables recorded concurrently with UAS image capture, five site-specific characteristics (Table 1) and two additional variables were derived (all site-level data is reported in Appendix A1).

Site characteristics

Towed video data were used to describe three site-specific parameters: density and patchiness of eelgrass; presence and density of non-eelgrass SAV species; and substrate tone, a subjective measure of sediment brightness based

Table 1. Environmental conditions and site-specific characteristics acquired or derived at each site, including the units or categories used to measure them.

Environmental characteristics	Method of derivation	Site-specific characteristics	Method of derivation
Tidal height	Government tide charts using time and location. Measured in meters (m).	Non-eelgrass SAV	Qualitative estimate derived from towed video. High, medium, and low suitability categories
Sun angle	Sun angle calculator (USNO, 2017) using time and site coordinates. Measured in degrees (°).	Eelgrass density	Qualitative estimate derived from towed video. High, medium, and low suitability categories
Wind speed	In field with handheld anemometer. Measured in kilometers per hour (km h^{-1}).	Substrate tone	Qualitative estimate derived from towed video. High, medium, and low suitability categories.
Secchi depth	In field with Secchi disk. Measured in meters (m)	Site exposure	ShoreZone exposure classifications. High, medium, and low suitability categories
Cloud cover	In field cover estimate with sky photos. Estimated in percent (%)	Eelgrass deep edge	Eelgrass delineation overlaid on bathymetric data. Measured in meters (m), negative when deep edge is below the zero (0 m) tide

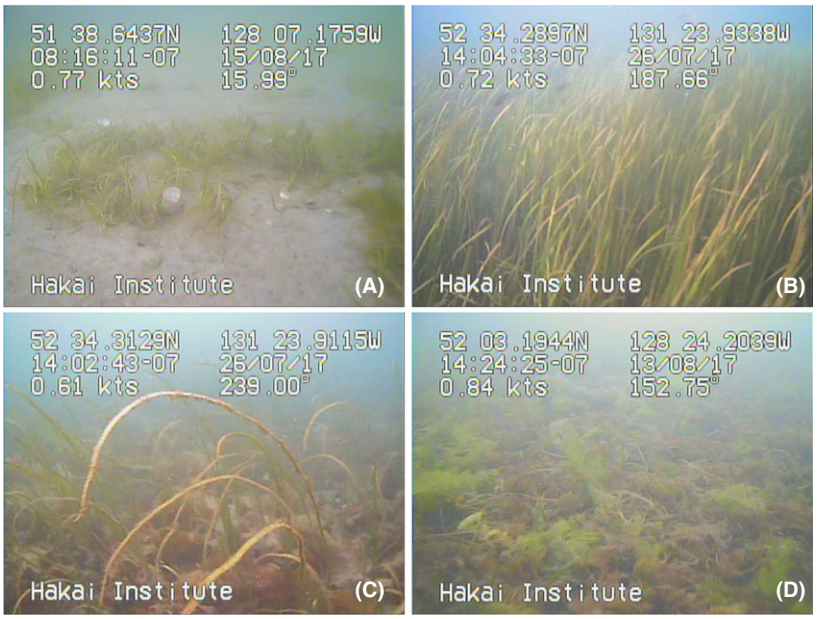

Figure 2. Examples of seagrass and non-seagrass SAV classifications from towed underwater video frames: (A) sparse eelgrass; (B) dense eelgrass; (C) mixed eelgrass with SAV; (D) dense SAV. Imagery is labeled with location, time, date, and speed information at time of acquisition.

on the range of tones present within the data. These three qualitative parameters were categorized by a single analyst based on their suitability for eelgrass mapping (High, Medium, or Low). High suitability characteristics included dense continuous eelgrass, sparse non-eelgrass SAV present (little to no intermixed algae), and bright sediments (high contrast with eelgrass). Low suitability characteristics included sparse patchy eelgrass, dense multi-species SAV present, and dark sediments (low contrast with eelgrass).

The eelgrass deep edge, defined as maximum bathymetric depth of eelgrass at each site, was determined by overlaying the delineated eelgrass polygon (section 2.5) on bathymetric data and extracting the maximum depth of each eelgrass bed. Bathymetric data (vector format) were obtained from the Canadian Hydrographic Service for all sites except those located in Haida Gwaii, which were provided by Parks Canada (raster format). The exposure of each site to wind and wave action was determined based on ShoreZone data, which provides classifications of linear units of shoreline in terms of sediment, biological attributes and exposure (Howes 2001; Shorezone, 2017). Six ShoreZone exposure categories were present among the sites, which were grouped into low, medium and high exposure categories for consistency with the other qualitative variables.

Derived wind ripple and theoretical visibility

The presence or absence of wind ripples was derived through visual inspection of the UAS imagery. In addition, the term 'theoretical visibility' (Equation 1) was created to describe the additive components of eelgrass deep edge, tidal height (referenced to chart datum; mean lower low water) (Fisheries and Oceans Canada, 2017), and Secchi depth on predictive detection of eelgrass. Theoretical visibility, measured in meters, describes how much "additional" visibility beyond the eelgrass deep edge is theoretically present. Positive values are indicative of a visible eelgrass deep edge, while negative values are indicative of a non-detectable deep edge. For example, an eelgrass meadow with deep edge at −2.5 m, with imagery collected at a 0.6 m tide and 3.5 m Secchi depth, would have 0.4 m of additional visibility beyond the deep eelgrass edge. In this case, theoretical visibility predicts that the deep edge of the bed should be visible in the image.

$$\begin{aligned}\text{Theoretical visibility} = {} & \text{Eelgrass deep edge (m)} \\ & - \text{tidal height (m)} \\ & + \text{Secchi depth (m)}\end{aligned} \quad (1)$$

UAS image processing and eelgrass delineation

Orthomosaics were produced using a Structure from Motion Multi-View Stereo (SfM-MVS) workflow within Pix4Dmapper software version 2.1.61, georeferenced to the GCPs surveyed in the field (Carrivick et al. 2016). The extent of eelgrass at each site was delineated from the

orthomosaics using object-based image analysis (OBIA) within eCognition Developer software (eCognition Developer 9, 2014). OBIA methods have been increasingly applied in order overcome issues associated with pixel-based classifiers for very high resolution imagery (Blaschke 2010). OBIA creates "image objects" through a segmentation process which splits the image into groups of pixels (i.e., image objects) which have uniform spectral and spatial characteristics (Baatz and Schape 2000). In this study, we used the multiresolution segmentation algorithm available within the eCognition framework. We determined image segmentation parameters (scale 50 and color 0.9) through experimentation to identify scale and color values that would be generally applicable across all sites. Following image segmentation (Fig. 3B), image objects were manually classified as eelgrass or non-eelgrass image objects based on the visual characteristics of the features (e.g., color and texture; Fig. 3C). While automated OBIA classification methods exist, we used manual classification of objects based on photointerpretive characteristics of the imagery due to varying radiometry across a site (Lathrop et al. 2006; Nahirnick et al. in press). Because image interpretation can be difficult in areas with sparse eelgrass, where eelgrass is intermixed with other macroalgae, or in areas of subtidal eelgrass, data from towed underwater video were used to aid image interpretation. For the 12 sites where accuracy assessments were conducted, only training data were used in image interpretation.

Confidence level and accuracy assessment

To describe the overall eelgrass mapping reliability, each site was assigned a mapping confidence level (MCL; low, medium or high) by consensus of two expert analysts, each with at least 4 years of research experience analyzing coastal aerial imagery (Table 2). A subset of 12 sites was chosen to be mapped by an additional independent analyst, including sites from each region and reflecting all mapping confidences from each region. For these 12 sites, ground reference data were split into training and validation datasets (70% and 30%, respectively) to conduct an accuracy assessment by using a modified error matrix (Congalton 1991). The size of the validation datasets ranged from 39 to 184 ground truth points depending on the site of the site.

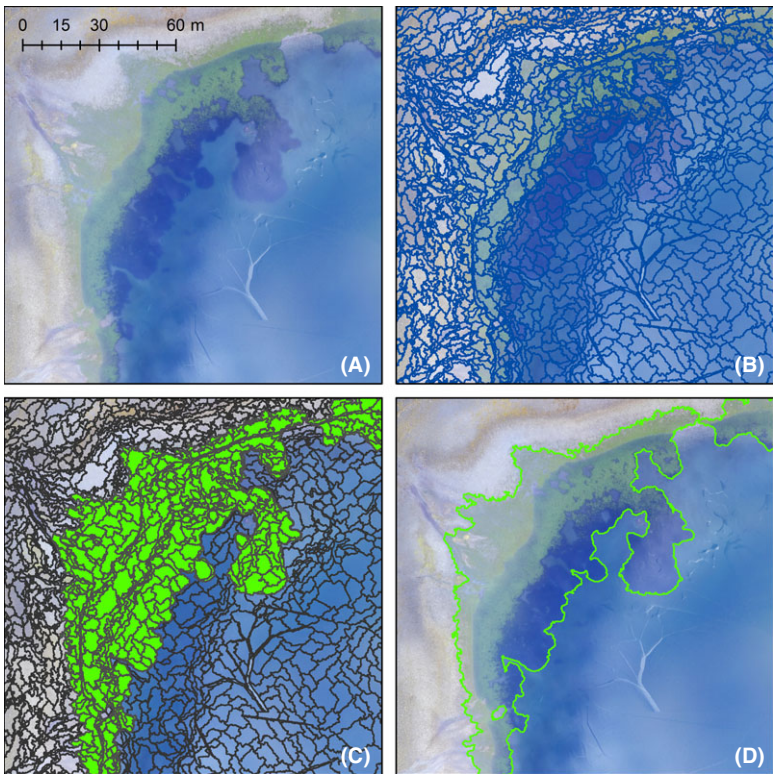

Figure 3. Example of eelgrass delineation process (site: Bag Harbour, GHNMCA): (A) original orthomosaic; (B) orthomosaic segmented into image objects; (C) image objects representing eelgrass manually selected based on photointerpretive characteristics; (D) classified image objects exported and merged to create final eelgrass delineation.

Table 2. Descriptions of mapping confidence level (MCL) categories assigned to each site

High Confidence	Medium Confidence	Low Confidence
Eelgrass extent was easy to delineate across the entire site. The eelgrass deep edge was easily detected. There was no confusion between eelgrass and other submerged vegetation or background sediments	Some areas of eelgrass within the site were difficult to delineate. The eelgrass deep edge was unclear in portions of the orthomosaic. Eelgrass and other submerged vegetation or background sediments were sometimes difficult to differentiate	Difficult to delineate eelgrass in a large portion of the site, particularly at the eelgrass deep edge. Difficult to differentiate eelgrass from other SAV or background sediments

Table 3. Statistical results of the Robust Linear Regression based on z test of coefficients. Significant effects in bold.

Variable	Estimate	Std. Error	*Z* value	*P*-value
Sun angle	−0.398660	0.163814	−2.4336	**0.01495**
Cloud Cover (linear)	0.046338	0.671331	0.0690	0.94497
Cloud Cover (quadratic)	0.685631	0.680296	1.0078	0.31353
Wind speed	−0.156413	0.137267	−1.1395	0.25450
Theoretical Visibility	0.390033	0.162916	2.3941	**0.01666**
EG patchiness	0.244811	0.176168	1.3896	0.16464
SAV mixing	0.077153	0.168981	0.4566	0.64797

Multivariate analysis

We used Robust Linear Regression to examine which factors were most important in determining eelgrass mapping confidence (i.e., MCL). All data analyses were performed using R version 3.4.4 (R Core Team, 2018). Environmental and site variables that exhibited multicollinearity were first identified and removed from the analysis based on their variance inflation factor, using the function vif from the MASS package (Venables and Ripley 2002). Variables that were removed were: Secchi depth, tidal height, and eelgrass deep edge (accounted for within theoretical visibility); substrate tone (subjective nature of tone categorization); and wind ripples and exposure (related to wind speed). The final set of predictor variables consisted of: sun angle, cloud cover, wind speed, theoretical visibility, eelgrass patchiness and density, and SAV presence and density. The reduced set of predictors were not significantly spatially autocorrelated (Moran's I test), and were near-normal, but visual examination of diagnostic plots suggested the presence of both high-leverage outliers and heteroskedasticity. The final predictor set was regressed on eelgrass MCL using Robust Linear Regression, which is robust to the presence of outliers (McKean 2004), using the rlm function from the MASS package (Venables and Ripley 2002). Because standard errors are typically biased by the presence of heteroskedasticity, heteroskedasticity-consistent standard errors were calculated using the vcovHC function from the sandwich package (Zeileis 2004).

Results

Multivariate analysis

Sun angle and theoretical visibility were the strongest predictors of assigned MCL (Table 3; $P < 0.05$). The other variables (Table 3: cloud cover, wind speed, eelgrass patchiness, SAV mixing) were not strong predictors of MCL; with variable standardized effects sizes. The larger standardized effect size and greater significance of the quadratic term for cloud cover, compared to the linear term, indicates that optimal cloud cover conditions occur at the very low and very high cloud covers. Of the eelgrass meadow characteristics, patchiness was a stronger predictor of mapping confidence than SAV mixing (Table 3; greater effect size and level of significance).

Confidence associated with environmental and site variables

Mapping confidence was explored in relation to each environmental and site characteristic (Fig. 4). UAS imagery collected at sun angles as low as 6.5° achieved high MCL, whereas a sun angle maximum of 40° resulted in a shift to low MCL (Fig. 4A). Tidal height did not exhibit a relationship with MCL (Fig. 4B), but high MCL was achieved at Secchi depths greater than 5 m (Fig. 4D). A wide range of cloud cover achieved high MCL (Fig. 4C). MCL decreased with increasing wind speed (Fig. 4E), with wind ripples observed at speeds greater than 8 km h^{-1} (Fig. 5a).

Differences in site characteristics resulted in changes in mapping confidence, except for the deep edge of the seagrass bed. Continuous dense (high suitability) eelgrass meadows achieved high MCL (Fig. 4F). In the low MCL category, the majority of sites were those with sparse patchy or mixed density eelgrass (low suitability). The majority of high MCL sites had sparse or moderate SAV mixing (high or medium suitability), while the proportion of dense and moderate SAV (medium or low suitability) sites increased in the low MCL category (Fig. 4G). Substrate tone also exhibited a relationship to MCL, where darker substrates (low suitability) achieved higher MCL than sites with brighter substrates (high suitability) (Fig. 4H). High MCL sites also had very low exposure (i.e., highly protected; high suitability) (Fig. 4I).

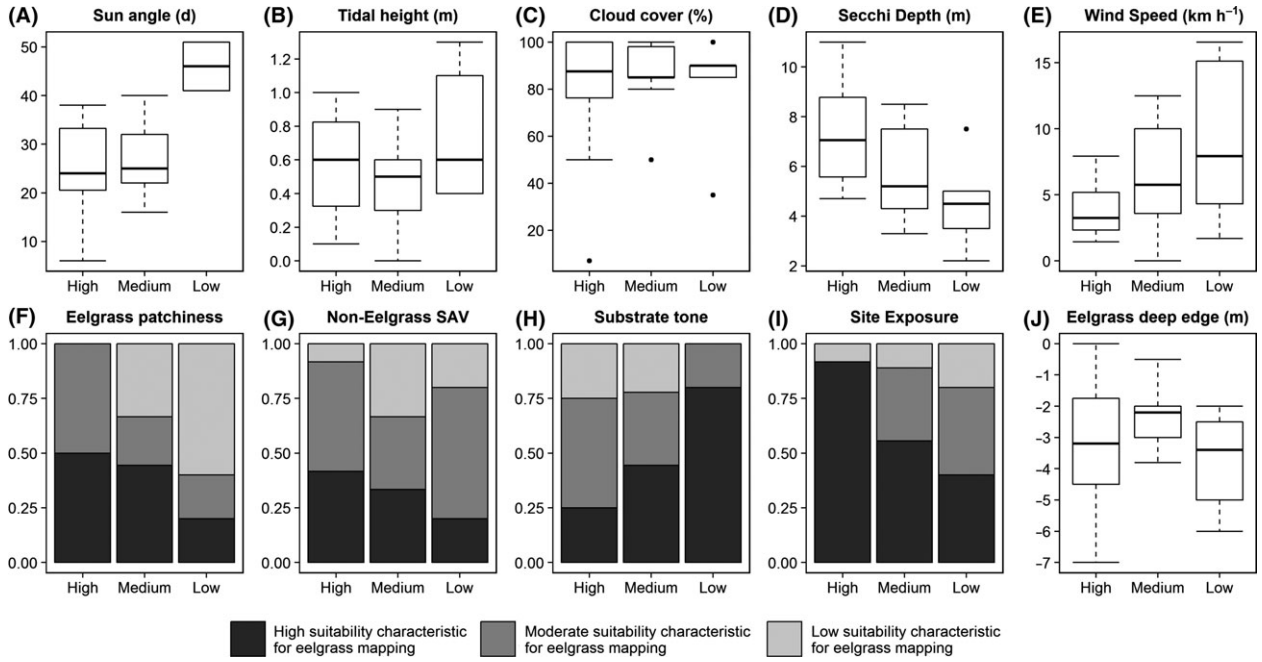

Figure 4. Environmental conditions (A–E) and site characteristics (F–J) plotted on the *y*-axis against Mapping Confidence Level across all *x*-axes (High, Medium, or Low confidence in eelgrass mapping output). For quantitative environmental or site characteristics, the center line of the boxplot represents the median, and the whiskers extend 1.5 times the interquartile range above and below the upper and lower quartile. For qualitative site characteristics, the right-hand y-axis represents the proportion of sites in each confidence level category. Raw data is provided in Appendix A1.

While Secchi depth showed a clear relationship to MCL, tidal height and eelgrass deep edge (Fig. 4J) did not. Combining these factors, reduced theoretical visibility (m) decreased mapping confidence (Fig. 5B). All high MCL sites were greater than 0 m, whereas all low MCL sites had negative or low (<1.25 m) theoretical visibility values.

Accuracy assessment

An accuracy assessment was conducted on a subset of 12 sites. High and medium MCL were associated with high overall accuracies, whereas low MCL overlapped with a larger range of accuracies (Fig. 6). The accuracy assessment, viewed as a cumulative error matrix (Table 4), showed that Producer's accuracy decreases with declining eelgrass density, while non-eelgrass cover types achieve high Producer's accuracies (>90%) in all categories.

Discussion

In this study, environmental conditions (i.e., sun angle) and their interactions with site characteristics (i.e., theoretical visibility) were both strong predictors of seagrass map confidence. Site characteristics (e.g., eelgrass density, presence of other SAV) were less important predictors of mapping outcomes. These results indicate that even complex, "less than ideal" sites (with regard to seagrass and SAV characteristics) can be mapped confidently if the imagery is acquired under optimal environmental conditions (Table 5). Herein, we highlight the most important factors affecting the confidence of an analyst to delineate the extent of eelgrass in UAS imagery, and review the limits of specific variables for reliable mapping.

Best predictors of UAS mapping outcome

Sun angle was the most important predictor of mapping confidence (Table 3). Recommendations for imagery acquisition of benthic habitats with piloted aircraft include sun angles between 15° and 45° (Dobson et al., 1996; Finkbeiner et al. 2001). However, we show that UAS may be able to achieve good quality imagery for benthic habitat mapping at lower sun altitudes with less illumination because the sensor is closer to the target than when using piloted aircraft. For temperate regions, our results indicate that high to medium mapping confidence is possible between sun angles of 6.5° to 40° (Fig. 4A), however, once sun angle exceeds 40°, confidence decreases (Fig. 7A and B). As predicted, sun angle, an environmental constraint on image quality, was an important predictor of mapping confidence.

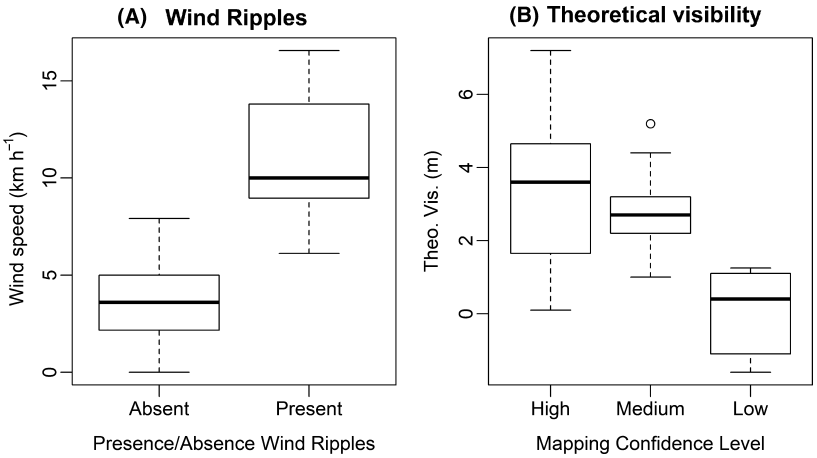

Figure 5. Additional variables, (A) presence or absence of wind ripples; (B) calculated theoretical visibility.

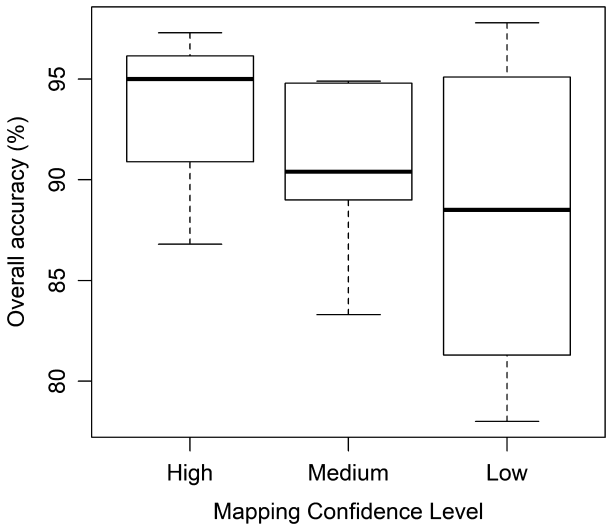

Figure 6. Overall accuracy (subset 12 sites) vs confidence levels assigned by analyst.

Also as anticipated, an interaction of environmental conditions and site characteristics (i.e., theoretical visibility) resulted in the second strongest predictor of UAS eelgrass mapping confidence (Table 3). While lower tidal heights offered slight improvements on mapping of submerged features (Fig. 4B), we demonstrate that tidal height interacts with local seagrass bed characteristics (i.e., how deep the eelgrass extends) and environmental conditions (i.e., water clarity at the time of acquisition) to determine the theoretical visibility for optimal mapping (Table 5). Unlike tropical regions where turbidity is generally low (Casella et al. 2016; Ventura et al., 2016), in temperate regions water clarity is a limiting factor in benthic habitat mapping (O'Neill et al. 2011) due to the presence of suspended material (organic detritus and inorganic sediments), phytoplankton, and CDOM causing reduced benthic visibility as is characterized by smaller Secchi depths (Babin et al., 2003; Dekker et al., 2006). When possible, mapping should be conducted during the lowest tides when turbidity levels are likely to be low (Fig. 7C and D). In addition, for site selection, incorporating a priori information on seagrass depth and turbidity (Thom et al., 2008) to calculate metrics of theoretical visibility can inform prioritization of mapping sites, based on optimal conditions.

Additional influences on mapping outcome

Contrary to our predictions, other seagrass bed characteristics (i.e., density and patchiness, SAV mixing) did not have strong effects on mapping confidence. Eelgrass

Table 4. Cumulative error matrix for subset of 12 sites. Accuracy is reported on an eelgrass presence or absence basis as delineated from the UAS orthomosaic.

	Habitat classes (number of samples)								
Eelgrass delineated in UAS image	Dense eelgrass	Moderate Eelgrass	Sparse eelgrass	Very sparse eelgrass	Brown Algae	Green Algae	Red Algae	Unvegetated	User's Accuracy
Eelgrass present	288	95	85	49	12	3	7	20	90.1%
Eelgrass absent	7	9	16	21	152	73	63	221	92.4%
Producer's Accuracy (%)	97.6%	91.3%	84.2%	70.0%	92.7%	96.1%	90.0%	91.7%	91.5%

Gray shaded boxes indicate the number of samples that were correctly classified, while the blue shaded box represents the overall accuracy.

Table 5. Optimal environmental conditions and site characteristics for mapping submerged eelgrass habitats.

Variable	Optimal conditions
Sun angle	6.5°–40°
Theoretical visibility	>0 m (low tide, low turbidity)
Cloud cover	0–10% or 90–100%
Wind	<8 km h^{-1}
Eelgrass meadow	Dense, continuous
SAV mixing	Sparse

patchiness was moderately important (Table 3, Table 4; decreasing Producer's accuracy as eelgrass density decreases), similar to other remote sensing studies of seagrass (Lathrop et al. 2006; Knudby & Norlund 2011; Reshitnyk et al. 2014). However, eelgrass patchiness was relatively more important than presence and density of non-eelgrass SAV (Table 3, Table 4; high accuracies of all non-eelgrass classes). While spectral similarity between eelgrass and other SAV species often results in mapping errors (Knudby & Norlund 2011; O'Neill et al. 2011; O'Neill and Costa 2013; Reshitnyk et al. 2014), textural characteristics present in the high spatial resolution UAS imagery may help distinguish between the two classes and improve mapping confidence in comparison to other remote sensing platforms (Bryson et al., 2013; Nahirnick et al. in press; Fig. 8A and B). Our accuracy assessment indicated that UAS imagery is more prone to underestimating eelgrass cover through the omission of sparse eelgrass areas than overestimation through the commission of non-eelgrass SAV (Table 3). Dense macroalgae exhibits textural differences that are generally distinguishable from dense eelgrass, whereas sparse eelgrass can easily be mistaken for sparse macroalgae, especially in areas where eelgrass is mixed with non-eelgrass SAV. The omission of sparse eelgrass is a common issue in classification of optical imagery (e.g., Barrell and Grant 2015) , and it may be possible to reduce this issue by: obtaining finer resolution imagery at lower flight altitudes; using pixel-based instead of object-based classifications in cases where there is minimal non-eelgrass SAV mixing (Duffy et al. 2018); or through the use of multispectral sensors mounted on UAS to utilize the spectral differences between eelgrass and macroalgae (O'Neill et al. 2011; Komárek et al. 2018).

Cloud cover was not amongst the top predictors of mapping confidence as we hypothesized. Rather, cloud cover and wind speed had comparable effects on mapping outcomes (Table 3). One of the benefits of using UAS for aerial imagery collection is the ability to fly in cloudy

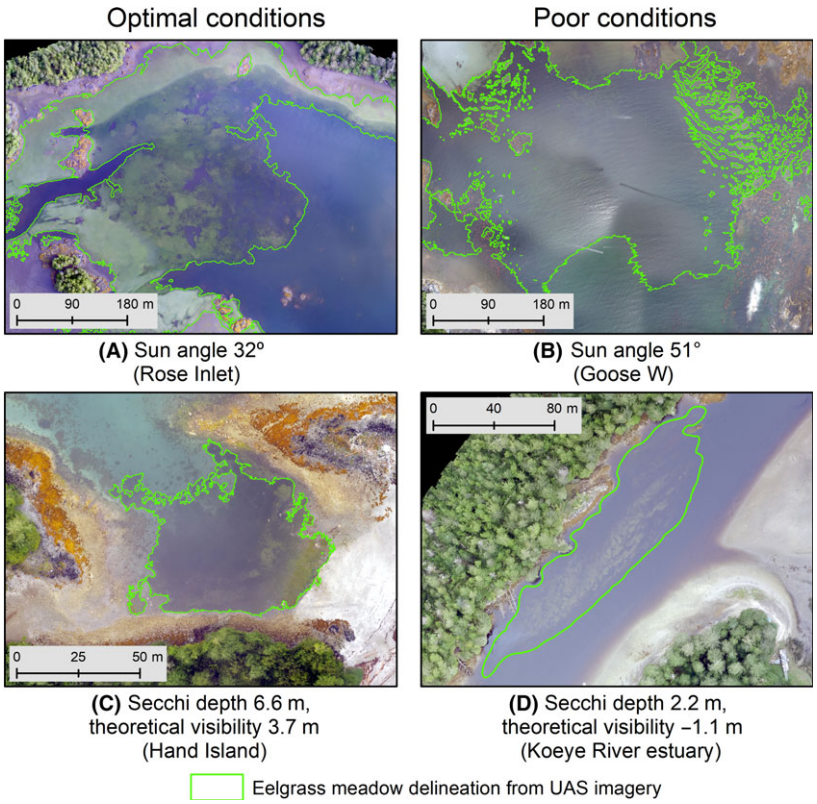

Figure 7. Visual comparisons of sites with optimal and poor sun angle (A and B) and water clarity (C and D) conditions.

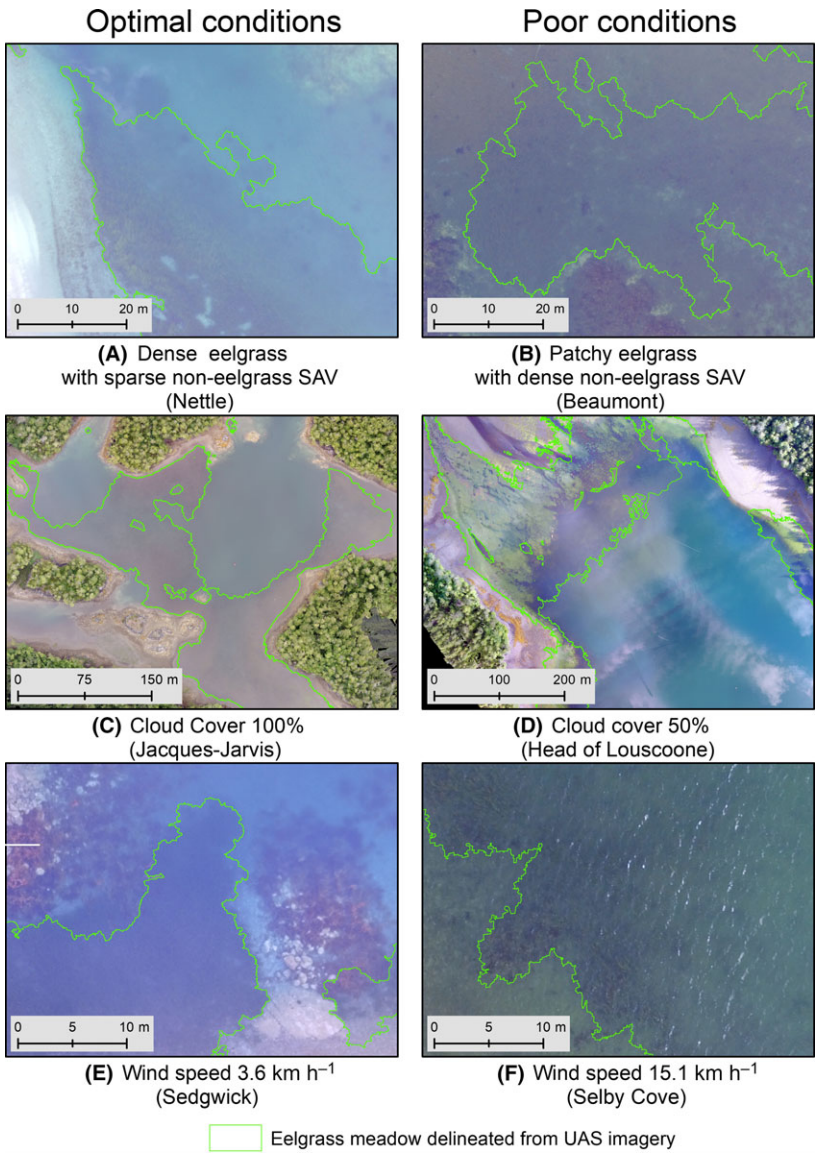

Figure 8. Visual comparisons of sites with optimal and poor conditions in terms of eelgrass density and non-eelgrass SAV presence (A and B), cloud cover (C and D), and wind speed (E and F) conditions.

conditions (for terrestrial examples see: Rango et al. 2009; Getzin et al. 2012; Bendig et al. 2014). However, when working with submerged features, cloud cover will impact the radiometric consistency of the imagery through the reflectance of clouds from the surface of the water (Duffy et al. 2017; Nahirnick et al. in press). Our results indicated that optimal cloud cover conditions are either very low (<10%) or very high (>90%) (Table 5), which provides consistent reflectance and radiometry (Nahirnick et al. in press; Fig. 8C and D). Recommended wind speeds for piloted aerial photography are <16 km h^{-1} (Dobson et al., 1996), with optimal imagery collected at wind speeds from 0 to 8 km h^{-1}. These recommendations are consistent with the results of this analysis, where high mapping confidence was possible with wind speeds up to 8 km h^{-1} (Fig. 8E and F). However, wind speeds between 5 km h^{-1} and 8 km h^{-1} may result in wind ripples depending on the angle of the sun (Mount 2005).

Two site-level characteristics, sediment tone and site exposure, were expected to alter mapping confidence, but were not included in the comparative analysis either because of an issue with the method of measurement, or because of correlation with another variable included in the analysis. It was expected that brighter sediments would result in greater mapping confidence due to the increased visual contrast between eelgrass and background sediments

(Pasqualini et al. 1997; Lathrop et al. 2006; O'Neill et al. 2011). However, the opposite trend was observed (Fig. 4H). This may be a result of the qualitative classification of sediment tone, which can change depending on illumination, and the possibility that the sites mapped in this study did not have a large enough gradient in substrate tone to observe an effect on mapping confidence. Consistent with expectations, almost all high MCL sites were located in the high protection category. Exposure is a problematic variable for prediction of mapping output as it may be correlated with other conditions, such as wind speeds creating ripple effects as well as site-level seagrass characteristics (e.g., seagrass cover and configuration; Fonseca and Bell 1998). As such, only wind speed was included in the multivariate analysis. However, site exposure remains an important factor to consider when planning data collection because of its potential to influence local wind speed and seagrass bed characteristics.

Improving map reliability

The relationships between environmental conditions, seagrass characteristics and other local site characteristics on UAS mapping outcomes were based on a large dataset of seagrass UAS maps delineating site-level seagrass presence-absence (26 sites; Appendix A1). Even so, analytical limitations did not allow examination of all possible scenarios. For example, most of the cloud cover conditions observed were in the 90–100% range, with far fewer in the low and middle range of cloud cover. Further, all low MCL sites had both sun angles above 40° and low theoretical visibility (<1.25 m). Future work could focus on exploring the full gradient of each variable on mapping confidence in order to assess some of the scenarios that were not captured in the present study, such as data acquisition with sun angles above 40° but with high theoretical visibility (>1.25 m). In addition, because of the fine scale resolution of UAS imagery, it has the ability to capture fine scale landscape characteristics (i.e., patch-gap patterns) in seagrass beds. In fact, some of these patterns emerged through our OBIA classifications (e.g., Fig. 7B). However, additional analyses are necessary to determine if the characteristics that emerged as important for total extent mapping are consistent with those for capturing eelgrass landscape features.

We assessed mapping reliability using two approaches. The traditional accuracy assessment indicated decreasing accuracy with decreasing eelgrass density, as expected, but did not reflect the analysts' assessment of the quality of imagery or their confidence in the mapping outputs. In order to provide another metric of mapping reliability, mapping confidence level categories were also used. This approach provided an expert elicitation of the quality of the imagery itself for deriving reliable eelgrass maps. Mapping confidence was positively related to mapping accuracy (Fig. 6) and improved our understanding of the environmental factors and site characteristics that impact mapping confidence (Fig. 4). While the results presented here have specifically addressed UAS eelgrass mapping in a temperate environment, the findings would be generally applicable to other submerged marine habitats such as macroalgae, rocky and biogenic reefs, and other seagrass species in both temperate and tropical environments (Casella et al. 2017; Ventura et al. 2018).

Conclusion

The spatial extent of eelgrass at 26 sites in British Columbia, Canada, was delineated in UAS orthomosaics using OBIA methods combining image segmentation with manual classification. Maps were then ranked according to confidence level by expert analysts. Sun angle and theoretical visibility were the two most important factors influencing mapping confidence of submerged eelgrass habitats in this temperate marine region. However, sites with "less than ideal" conditions (e.g., sparse eelgrass cover, presence and mixing of other SAV) can also be mapped with high confidence using UAS technology when suitable environmental conditions are present. Research on UAS applications for nearshore marine habitats has focused on exposed intertidal temperate areas or clear tropical waters. Here, the variable environmental conditions and site characteristics pertinent to seagrass subtidal components in temperate regions were evaluated to provide guidance for future application of this technology by coastal managers, scientists and practitioners. UAS imagery provides an accurate and cost-effective tool to monitor temperate eelgrass meadows, detect change in eelgrass habitat extent and configuration, and contribute to effective protection and restoration actions for this vital nearshore ecosystem.

Acknowledgments

This research was jointly supported by the Tula Foundation (Hakai Institute), Parks Canada, University of Victoria and Mitacs (Grant #IT07414). Field work and imagery acquisition was conducted in partnership with the Hakai Institute, Parks Canada and local First Nations communities. The authors acknowledge the multiple First Nation territories in which the data were collected. Many thanks to colleagues and field assistants at all participating organizations in the collection of the field data: Will Hall, Derek Heathfield, Keith Holmes, Will McInnes, Tara Sharma, Mike Vegh, Rebecca Holte, Christine Bentley, Niisii Guujaaw, Clint Johnson Kendrick, Cameron Sanjivi,

Caron Olive, Dan Grinnell, Mike Wald, Sarah Brittain and Teagan O'Shaughnessy.

References

Anderson, K., and K. J. Gaston. 2013. Lightweight unmanned aerial vehicles will revolutionize spatial ecology. *Front. Ecol. Environ.* **11**(3), 138–146.

Baatz, M., and A. Schape. 2000. Multiresolution Segmentation: an Optimization Approach for High Quality Multi-Scale Image Segmentation. Pp. 12–23 in J. Strobl, T. Blaschke and G. Griesebner, eds. *Angewandte geographische informations-verarbeitung*, 7th ed.. Wichmann Verlag, Karlsruhe, Germany.

Babin, M., A. Morel, V. Fournier-Sicre, F. Fell, and D. Stramski. 2003. Light scattering properties of marine particles in coastal and open ocean waters as related to the particle mass concentration. *Limnol. Oceanogr.* **48**(2), 843–859.

Barrell, J., and J. Grant. 2015. High-resolution, low altitude aerial photography in physical geography: a case study characterizing eelgrass (*Zostera marina L.*) and blue mussel (*Mytilus edulis L.*) landscape mosaic structure. *Prog. Phys. Geogr.* **39**(4), 440–459.

Beck, M. W., K. L. Heck, K. W. Able, D. L. Childers, D. B. Eggleston, B. M. Gillanders, et al. 2001. The identification, conservation, and management of estuarine and marine nurseries for fish and invertebrates. *Bioscience* **51**(8), 633–641.

Bendig, J., A. Bolten, S. Bennertz, J. Broscheit, S. Eichfuss, and G. Bareth. 2014. Estimating biomass of barley using crop surface models (CSMs) derived from UAV-based RGB imaging. *Remote Sens.* **6**, 10395–10412.

Blaschke, T. 2010. Object based image analysis for remote sensing. *ISPRS J. Photogramm. Remote Sens.* **65**, 2–16.

Bostrom, C., S. J. Pittman, C. Simenstad, and R. T. Kneib. 2011. Seascape ecology of coastal biogenic habitats: advances, gaps, and challenges. *Mar. Ecol. Prog. Ser.* **427**, 191–217.

Bryson, M., M. Johnson-Roberson, R. J. Murphy, and D. Bongiorno. 2013. Kite aerial photography for low-cost, ultra-high spatial resolution multi-spectral mapping of intertidal landscapes. *PLoS ONE*, **8**(9), 1–15.

Carrivick, J. L., M. W. Smith, and D. J. Quincey. 2016. P. 208*Structure from motion in the geosciences*. Wiley-Blackwell, Oxford, UK.

Casella, E., A. Rovere, A. Pedroncini, C. P. Stark, M. Casella, M. Ferrari, et al. 2016. Drones as tools for monitoring beach topography changes in the Ligurian Sea (NW Mediterranean). *Geo-Mar. Lett.* **36**, 151–163.

Casella, E., A. Collin, D. Harris, S. Ferse, S. Bejarano, V. Parravicini, et al. 2017. Mapping coral reefs using consumer-grade drones and structure from motion photogrammetry techniques. *Coral Reefs* **36**, 269–275.

Congalton, R. G. 1991. A review of assessing the accuracy of classifications of remotely sensed data. *Remote Sens. Environ.* **37**, 35–46.

Costanza, R., R. D'Arge, R. de Groot, S. Farber, M. Grasso, B. Hannon, et al. 1997. The value of the world's ecosystem services and natural capital. *Nature* **387**(15), 253–260.

Dekker, A., V. Brando, J. Anstee, S. Fyfe, T. Malthus, and E. Karpouzli. 2006. Remote sensing of seagrass ecosystems: use of spaceborne and airborne sensors. Pp. 347–359 in A. W. D. Larkum, R. J. Orth and C. M. Duarte, eds. *Seagrasses: biology, ecology, and conservation*. Springer, Dordrecht.

Dobson, J. E., E. A. Bright, R. L. Ferguson, D. W. Field, L. L. Wood, K. D. Haddad, et al. (1996). *Monitoring Submerged Land Using Aerial Photography. NOAA Coastal Change Analysis Program (C-CAP)*. NOAA technical report NMFS 123.

Duffy, J. P., A. M. Cunliffe, L. DeBell, C. Sandbrook, S. A. Wich, J. D. Shutler, et al. 2017. Location, location, location: considerations when using lightweight drones in challenging environments. *Remote Sens. Ecol. Conserv.* **4**, 7–19.

Duffy, J. P., L. Pratt, K. Anderson, P. E. Land, and J. D. Shutler. 2018. Spatial assessment of intertidal seagrass meadows using optical imaging systems and a lightweight drone. *Estuar. Coast. Shelf Sci.* **200**, 169–180.

Finkbeiner, M., B. Stevenson, and R. Seaman. 2001. *Guidance for Benthic Habitat Mapping: An Aerial Photographic Approach*. NOAA Coastal Services Center.

Fisheries and Oceans Canada. 2017. *Tides, Currents, and Water Levels*. Accessed online at www.tides.gc.ca

Fonseca, M., and S. Bell. 1998. Influence of physical setting on seagrass landscapes near Beaufort, North Carolina, USA. *Mar. Ecol. Prog. Ser.* **171**, 109–121.

Getzin, S., K. Wiegand, and I. Schoning. 2012. Assessing biodiversity in forests using very high-resolution images and unmanned aerial vehicles. *Methods Ecol. Evol.* **3**, 397–404.

Green, E. P., P. J. Mumby, A. J. Edwards, and C. D. Clark. 2000. *Remote sensing handbook for tropical coastal management*. UNESCO, Paris.

Hansen, J. C. R., and M. A. Reidenbach. 2013. Seasonal growth and senescence of a *Zostera marina* Seagrass meadow alters wave-dominated flow and sediment suspension within a Coastal Bay. *Estuaries Coasts* **36**, 1099–1114.

Hogrefe, K., D. Ward, T. Donnelly, and N. Dau. 2014. Establishing a baseline for regional scale monitoring of eelgrass (*Zostera marina*) habitat on the lower Alaska Peninsula. *Remote Sens.* **6**, 12447–12477.

Hossain, M. S., J. S. Bujang, M. H. Zakaria, and M. Hashim. 2015. The application of remote sensing to seagrass ecosystems: an overview and future research prospects. *Int. J. Remote Sens.* **36**(1), 61–114.

Howes, D. E. 2001. BC Biophysical Shore-Zone Mapping System – A Systematic Approach to Characterize Coastal Habitats in the Pacific Northwest. Puget Sound Research Conference, p. 11.

Johnston, D. W. 2019. Unoccupied aircraft systems in marine science and conservation. *Annu. Rev. Mar. Sci.*, **11**, 1–25. https://doi.org/10.1146/annurev-marine-010318-095323

Klemas, V. 2015. Coastal and environmental remote sensing from unmanned aerial vehicles: an overview. *J. Coastal Res.* **31**(5), 1260–1267.

Klemas, V. 2016. Remote Sensing of Submerged Aquatic Vegetation. Pp. 125–140 in C. W. Finkl, C. Makowski, eds. *Seafloor mapping along continental shelves: research and techniques for visualizing benthic environments* (13th ed.). Coastal Research Library, Switzerland, Springer.

Knudby, A., and L. Nordlund. 2011. Remote sensing of seagrasses in a patchy multi-species environment. *Int. J. Remote Sens.* **32**(8), 2227–2244.

Komárek, J., T. Klouček, and J. Prošek. 2018. The potential of unmanned aerial systems: a tool towards precision classification of hard-to-distinguish vegetation types? *Int. J. Appl. Earth Obs. Geoinf.* **71**, 9–19.

Larkum, A. W. D., R. J. Orth, and C. M. Duarte. 2007. *Seagrasses: biology, ecology, and conservation*. Springer, Dordrecht, The Netherlands.

Lathrop, R. G., P. Montesano, and S. Haag. 2006. A multi-scale segmentation approach to mapping seagrass habitats using airborne digital camera imagery. *Photogramm. Eng. Remote Sensing* **72**(6), 665–675.

Manfreda, S., M. F. McCabe, P. E. Miller, R. Lucas, V. M. Pajuelo, G. Mallinis, et al. 2018. Use of unmanned aerial systems for environmental monitoring. *Remote Sens.* **10**(4), 641.

Martínez-Carricondo, P., F. Agüera-Vega, F. Carvajal-Ramírez, F.-J. Mesas-Carrascosa, A. García-Ferrer, and F.-J. Pérez-Porras. 2018. Assessment of UAV-photogrammetric mapping accuracy based on variation of ground control points. *Int. J. Appl. Earth Obs. Geoinf.* **72**, 1–10.

McKean, J. W. 2004. Robust analysis of linear models. *Stat. Sci.* **19**(4), 562–570.

Mount, R. 2005. Acquisition of through-water aerial survey images: surface effects and the prediction of sun glitter and subsurface illumination. *Photogramm. Eng. Remote Sensing* **71**(12), 1407–1415.

Nahirnick, N., P. Hunter, M. Costa, S. Schroeder, and T. Sharma. (in press). Benefits and challenges of UAS imagery for eelgrass (*Zostera marina*) mapping in small estuaries of the Salish Sea. *J. Coastal Res.*

O'Neill, J. D., and M. Costa. 2013. Mapping eelgrass (*Zostera marina*) in the Gulf Islands National Park Reserve of Canada using high spatial resolution satellite and airborne imagery. *Remote Sens. Environ.* **133**, 152–167.

O'Neill, J. D., M. Costa, and T. Sharma. 2011. Remote sensing of shallow coastal benthic substrates: in situ spectra and mapping of eelgrass (*Zostera marina*) in the Gulf Islands National Park Reserve of Canada. *Remote Sens.* **3**, 975–1005.

Orth, R. J., T. J. B. Carruthers, W. C. Dennison, C. M. Duarte, J. W. Fourqurean, K. L. Heck, et al. 2006. A global crisis for seagrass ecosystems. *Bioscience* **56**(12), 987–996.

Pasqualini, V., C. Pergent-Martini, C. Fernandez, and G. Pergent. 1997. The use of airborne remote sensing for benthic cartography: advantages and reliability. *Int. J. Remote Sens.* **18**(5), 1167–1177.

Phillips, R. C. 1984. *The ecology of eelgrass meadows in the Pacific Northwest: A community profile*. U.S. Fish and Wildlife Service.

Plummer, M. L., C. J. Harvey, L. E. Anderson, A. D. Guerry, and M. H. Ruckelshaus. 2013. The role of eelgrass in marine community interactions and ecosystem services: results from ecosystem-scale food web models. *Ecosystems* **16**, 237–251.

R Core Team. 2018. *R: a language and environment for statistical computing*. R Foundation for Statistical Computing, Vienna, Austria. Version 3.4.4

Rango, A., A. Laliberte, J. E. Herrick, C. Winters, K. Havstad, C. Steele, et al. 2009. Unmanned aerial vehicle-based remote sensing for rangeland assessment, monitoring, and management. *J. Appl. Remote Sens.* **3**(1), 1–15.

Reshitnyk, L., C. L. K. Robinson, and P. Dearden. 2014. Evaluation of WorldView-2 and acoustic remote sensing for mapping benthic habitats in temperate coastal Pacific waters. *Remote Sens. Environ.* **153**, 7–23.

Shorezone. 2017. Accessed September 2017: www.shorezone.org

Short, F. T., and S. Wyllie-Echeverria. 1996. Natural and human-induced disturbance of seagrasses. *Environ. Conserv.* **23**(1), 17–27.

Singh, K. K., and A. E. Frazier. 2018. A meta-analysis and review of unmanned aircraft system (UAS) imagery for terrestrial applications. *Int. J. Remote Sens.* **39**(15–16), 5078–5098.

Thom, R. M., S. L. Southard, A. B. Borde, and P. Stoltz. 2008. Light requirements for growth and survival of eelgrass (*Zostera marina* L.) in Pacific Northwest (USA) estuaries. *Estuaries Coasts* **31**(5), 969–980.

United States Naval Observatory (USNO). 2017. *Sun or Moon Altitude/Azimuth Table*. http://aa.usno.navy.mil/data/docs/AltAz.php

Venables, W. N., and B. D. Ripley. 2002. *Modern applied statistics with S*, 4th ed.. Springer, New York.

Ventura, D., M. Bruno, G. Jona, A. Belluscio, and G. Ardizzone. 2016. A low-cost drone based application for identifying and mapping of coastal fish nursery grounds. *Estuar. Coast. Shelf Sci.* **171**, 85–98.

Ventura, D., A. Bonifazi, M. F. Gravina, A. Belluscio, and G. Ardizzone. 2018. Mapping and classification of ecologically sensitive marine habitats using unmanned aerial vehicle (UAV) imagery and object-based image analysis (OBIA). *Remote Sens.* **10**(1331), 1–23.

Zeileis, A. 2004. Econometric computing with HC and HAC covariance matrix estimators. *J. Stat. Softw.* **11**(10), 1–17.

Supporting Information

Additional supporting information may be found online in the Supporting Information section at the end of the article.

Appendix A1: Dataset of environmental conditions and site characteristics at 26 sites around coastal British Columbia.

